INSTITUTE OF PHYSICS PUBLISHING JOURNAL OF PHYSICS G: NUCLEAR AND PARTICLE PHYSICS

J. Phys. G: Nucl. Part. Phys. **34** (2007) 1–25 doi:10.1088/0954-3899/34/1/001

Low-energy collisions of heavy nuclei: dynamics of sticking, mass transfer and fusion

Valery Zagrebaev[1] **and Walter Greiner**[2]

[1] Flerov Laboratory of Nuclear Reaction, JINR, Dubna, Moscow Region, Russia
[2] Frankfurt Institute for Advanced Studies, JW Goethe-Universität, Frankfurt, Germany

E-mail: valeri.zagrebaev@jinr.ru

Received 27 September 2006
Published 27 October 2006
Online at stacks.iop.org/JPhysG/34/1

Abstract

The dynamics of heavy-ion low-energy collisions is studied within the realistic model based on multi-dimensional Langevin equations. Interplay of strongly coupled deep inelastic scattering, quasi-fission and fusion–fission processes is discussed. Collisions of very heavy nuclei (^{238}U+^{238}U, ^{232}Th+^{250}Cf and ^{238}U+^{248}Cm) are investigated as an alternative way for the production of super-heavy elements with increasing neutron number. Large charge and mass transfer were found in these reactions due to the inverse (anti-symmetrizing) quasi-fission process leading to the formation of surviving super-heavy long-lived neutron-rich nuclei. In many events the lifetime of the composite giant system consisting of two touching nuclei turns out to be rather long ($\geqslant 10^{-20}$ s), sufficient for observing line structure in spontaneous positron emission from super-strong electric fields, a fundamental QED process.

Communicated by Professor H Stoecker

1. Introduction

The mechanism of strongly damped collisions between very heavy nuclei was studied extensively about twenty years ago (see, for example, review [1] and references therein). Among other topics, there had been great interest in the use of heavy-ion transfer reactions with actinide targets to produce new nuclear species in the transactinide region [2–7]. The cross sections were found to decrease very rapidly with increasing atomic number of surviving target-like fragments. However, Fm and Md neutron-rich isotopes have been produced at the level of 0.1 μb. It was observed also that nuclear structure (in particular, the closed neutron shell $N = 126$) may strongly influence nucleon flow in dissipative collisions with actinide targets [8].

Renewed interest from our side to collision of transactinide nuclei is conditioned by the necessity to clarify much better than before the dynamics of heavy nuclear systems at low excitation energies and by a search for new ways for the production of neutron-rich super-heavy (SH) nuclei and isotopes. SH elements obtained in 'cold' fusion reactions with Pb or Bi target [9] are situated along the proton drip line being very neutron-deficient with a short half-life. In fusion of actinides with ^{48}Ca more neutron-rich SH nuclei are produced [10] with much longer half-life. But they are still far from the centre of the predicted first 'island of stability' formed by the neutron shell around $N = 184$. In the 'cold' fusion, the cross sections for formation of SH nuclei decrease very fast with increasing charge of the projectile and become less than 1 pb for $Z \geqslant 112$. On the other hand, heaviest transactinide, Cf, which can be used as a target in the second method, leads to the SH nucleus with $Z = 118$ being fused with ^{48}Ca. Using the next nearest elements instead of ^{48}Ca (e.g., ^{50}Ti, ^{54}Cr, etc) in fusion reactions with actinides is expected less encouraging, though experiments of such kind are planned to be performed. In this connection other ways to the production of SH elements in the region of the 'island of stability' should be searched for.

At incident energies around the Coulomb barrier in the entrance channel the fusion probability is about 10^{-3} for mass asymmetric reactions induced by ^{48}Ca and much less for more symmetric combinations used in the 'cold synthesis'. Deep inelastic (DI) scattering and quasi-fission (QF) [11–13] are the main reaction channels here, whereas the fusion probability (formation of compound nucleus (CN)) is extremely small. Note that QF phenomena are revealed in, and could be important also for comparatively light fusing systems [13, 14]. It is the QF process that inhibits fusion by several orders of magnitude for heavy nuclear systems. To estimate such a small quantity for CN formation probability, first of all, one needs to be able to describe well the main reaction channels, namely DI and QF. Moreover, the quasi-fission processes are very often indistinguishable from the DI scattering and from regular fission, which is the main decay channel of excited heavy CN.

Recently a new model has been proposed [15] for simultaneous description of all these strongly coupled processes: DI scattering, QF, fusion and regular fission. In this paper, we develop further this model and apply it for analysis of low-energy dynamics of heavy nuclear systems formed in nucleus–nucleus collisions at the energies around the Coulomb barrier. Among others there is the purpose to find an influence of the shell structure of the driving potential (in particular, deep valley caused by the double shell closure $Z = 82$ and $N = 126$) on the formation of CN in mass asymmetric collisions and on nucleon rearrangement between primary fragments in more symmetric collisions of actinide nuclei. In the first case, discharge of the system into the lead valley (normal or symmetrizing quasi-fission) is the main reaction channel, which decreases significantly the probability of CN formation. In collisions of heavy transactinide nuclei (U+Cm, etc), we expect that the existence of this valley may notably increase the yield of surviving neutron-rich super-heavy nuclei complementary to the projectile-like fragments (PLF) around lead ('inverse' or anti-symmetrizing quasi-fission reaction mechanism).

Direct time analysis of the collision process allows us to estimate also the lifetime of the composite system consisting of two touching heavy nuclei with total charge $Z > 180$. Such 'long-living' configurations (if they exist) may lead to spontaneous positron emission from super-strong electric fields of giant quasi-atoms by a static QED process (transition from neutral to charged QED vacuum) [16, 17].

In section 2, we discuss the principal degrees of freedom, the multi-dimensional adiabatic potential energy surface and the corresponding time-dependent equations of motion which may be used for comprehensive analysis of low-energy dynamics of heavy nuclear systems formed in nucleus–nucleus collisions. In section 3, we analyse regularities of low-energy

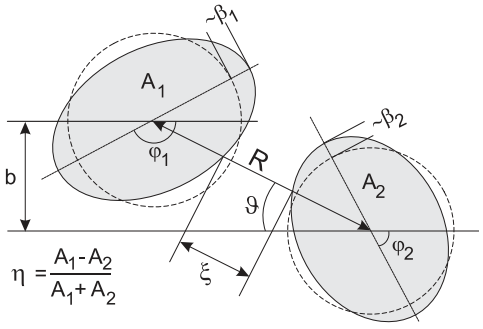

Figure 1. Degrees of freedom used in the model.

DI collisions of heavy nuclei comparing our calculations with experimental data. Regular (symmetrizing) QF phenomena and its influence on CN formation are also discussed in this section. In the last section the low-energy collisions of transactinide nuclei (^{238}U+^{238}U, ^{232}Th+^{250}Cf and ^{238}U+^{248}Cm) are investigated as an alternative way for the production of super-heavy elements. Lifetimes of the composite systems consisting of two touching nuclei are studied with the objective to find time delays suitable for the observation of spontaneous positron emission from super-strong electric field.

2. Adiabatic dynamics of heavy nuclear system

To describe properly and simultaneously the strongly coupled DI, QF and fusion–fission processes of low-energy heavy-ion collisions we have to choose, first, the unified set of degrees of freedom playing the principal role both at approaching stage and at the stage of separation of reaction fragments. The number of the degrees of freedom should not be too large so that one is able to solve numerically the corresponding set of dynamic equations. On the other hand, however, with a restricted number of collective variables it is difficult to describe simultaneously DI collision of two separated nuclei and QF of the highly deformed mono-nucleus. Second, we have to determine the unified potential energy surface (depending on all the degrees of freedom) which regulates in general all the processes. Finally, the corresponding equations of motion should be formulated to perform numerical analysis of the studied reactions.

Note that we take into consideration all the degrees of freedom needed for description of all the reaction stages (see below). Thus, in contrast with other models, we need not to split artificially the whole reaction into several stages when we consider strongly coupled DI, QF and CN formation processes. Moreover, in that case unambiguously defined initial conditions are easily formulated at large distance, where only the Coulomb interaction and zero-vibrations of the nuclei in their ground states determine the motion.

2.1. Degrees of freedom and potential energy surface

The distance between the nuclear centres R (corresponding to the elongation of a mono-nucleus), dynamic spheroidal-type surface deformations β_1 and β_2, mutual in-plane orientations of deformed nuclei φ_1 and φ_2, and mass asymmetry $\eta = \frac{A_1-A_2}{A_1+A_2}$ are probably the relevant degrees of freedom in fusion–fission dynamics. Taken together there are seven degrees of freedom as shown in figure 1. For the separation stage in the exit channel neck formation should be included to describe properly mass and energy distributions of the fission

fragments. To avoid increasing the number of degrees of freedom we take into account the necking process in a phenomenological way (see below).

The interaction potential of separated nuclei is calculated rather easily within the folding procedure with effective nucleon–nucleon interaction or parametrized, e.g., by the proximity potential [18]. Of course, some uncertainty remains here, but the height of the Coulomb barrier obtained in these models coincides with the empirical Bass parametrization [19] within 1 or 2 MeV. Dynamic deformations of colliding spherical nuclei and mutual orientation of statically deformed nuclei significantly affect their interaction changing the height of the Coulomb barrier for more than 10 MeV. It is caused mainly by a strong dependence of the distance between nuclear surfaces on the deformations and orientations of nuclei [20]. Geometrical effect due to a change in curvature of deformed nuclear surfaces is also important here [21, 22] and should be taken into account if the phenomenological nucleus–nucleus potential is used. An explicit formula for the geometrical factor for the interaction of deformed and rotated nuclei along with its simple parametrization (free from the unphysical singularity at zero curvature of flat surface) can be found in [22].

After contact the mechanism of interaction of two colliding nuclei becomes more complicated. For fast collisions ($E/A \sim \varepsilon_{\text{Fermi}}$ or higher) the nucleus–nucleus potential, V_{diab}, should reveal a strong repulsion at short distances protecting the 'frozen' nuclei to penetrate each other and form a nuclear matter with double density (diabatic conditions, sudden potential [23]). For slow collisions (near-barrier energies), when nucleons have enough time to reach equilibrium distribution (adiabatic conditions), the nucleus–nucleus potential energy, V_{adiab}, is quite different. Thus, for the nucleus–nucleus collisions at energies well above the Coulomb barrier we need to use a time-dependent potential energy, which after contact gradually transforms from a diabatic potential energy into an adiabatic one: $V = V_{\text{diab}}[1 - f(t)] + V_{\text{adiab}} f(t)$ [15, 24]. Here t is the time of interaction and $f(t)$ is a smoothing function with parameter $\tau_{\text{relax}} \sim 10^{-21}$ s, $f(t = 0) = 0$, $f(t \gg \tau_{\text{relax}}) = 1$. The calculation of the multi-dimensional adiabatic potential energy surface for heavy nuclear system remains a very complicated physical problem, which is not yet solved in full.

In figure 2, the amplitude of the wavefunction of valence neutron located initially in the $2d\frac{5}{2}$ state of ^{96}Zr nucleus is shown for the three different distances between colliding nuclei ^{40}Ca+^{96}Zr at near-barrier collision energy $E_{\text{c.m.}} = 97$ MeV. This wavefunction was obtained by the numerical solution of the three-body time-dependent Schrödinger equation [25]. As can be seen, the wavefunctions of valence neutrons follow the two-centre quasi-molecular states and spread over volumes of both nuclei rather fast, before nuclei come in contact and even before they overcome the Coulomb barrier. These microscopic quantum calculations confirm an important role of nucleon transfer and support the idea of nucleon collectivization [26, 27] in near-barrier fusion reactions.

In this connection the two-centre shell model [28] seems to be most appropriate for the calculation of the adiabatic potential energy surface. However, the simplest version of this model with restricted number of collective coordinates, using standard parametrization of the macroscopic (liquid drop) part of the total energy [29, 30] and overlapping oscillator potentials for the calculation of the single-particle states and resulting shell correction, does not reproduce correctly the values of the nucleus–nucleus interaction potential for well-separated nuclei and at contact point (depending on mass asymmetry). The same holds for the value of the Coulomb barrier and the depth of potential pocket at contact. No doubt, within an extended version of this model all these shortcomings may be overcome. We are currently working on this line.

Here we used the adiabatic potential energy of the nuclear system calculated within the semi-empirical two-core model of nucleon collectivization [26, 27] based on the two-centre shell model idea [28]. To get a reasonable value for the fission barrier, we used the

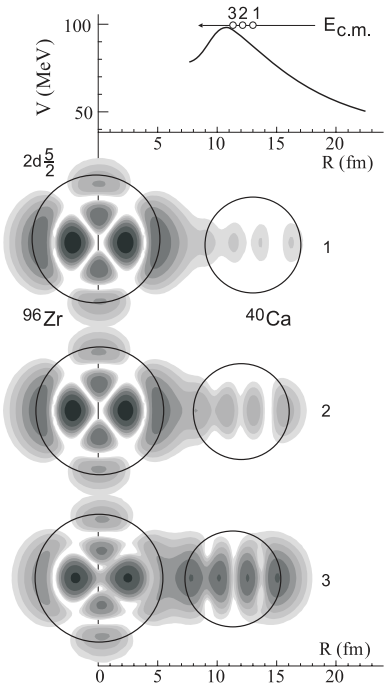

Figure 2. Amplitude of the wavefunction of valence neutron (initially located in the $2d\frac{5}{2}$ state of ^{96}Zr nucleus) at the three distances between colliding nuclei shown by the small circles in upper part of the figure along with the nucleus–nucleus potential energy.

shell corrections at zero and ground state deformations calculated according to [30] and the parametrization of the liquid drop energy proposed in [31]. Based on these values the adiabatic potential was calculated for small deformations. Then it was joined together with the potential of two touching nuclei as it was proposed in [26, 27]. Experimental binding energies of two cores are used here for the intermediate shapes, thus giving us the 'true' values of the shell corrections. As a result, the two-core model gives automatically an explicit (experimental) value of the nucleus–nucleus interaction energy in the asymptotic region for well-separated nuclei where it is known (the Coulomb interaction plus nuclear masses). It also gives quite realistic heights of the Coulomb barriers, that is very important for the description of near-barrier heavy-ion reactions. Note that the proposed driving potential is defined in the whole region $R_{\rm CN} < R < \infty$; it is a continuous function at $R = R_{\rm contact}(\eta, \beta_1, \beta_2)$ and, thus, may be used for simultaneous description of the whole fusion–fission process.

Found in such a way, the adiabatic potential is used further as a bottom value of the potential energy surface of the nuclear system in a space of collective degrees of freedom. Difference between total energy and a sum of this potential energy surface and kinetic energy is treated as an excitation energy of the nuclear system (its temperature). This excitation (gradually appearing when nuclei approach each other) leads to fluctuations of the collective degrees of freedom, which may be taken into account by the random forces within the Langevin type of equations of motion [32].

It is well known that the orientation effects play very important role in sub-barrier fusion of deformed nuclei by significantly increasing the capture probability due to decreasing the Coulomb barrier for nose-to-nose collisions (see, e.g., review paper [33]). There is some

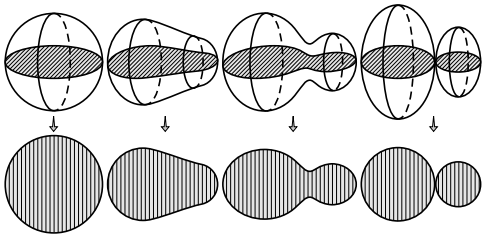

Figure 3. Back and top views (upper and bottom figures) of subsequent shapes of the nuclear system evolving from the configuration of two equatorially touching statically deformed nuclei to the configuration of spherical CN.

evidence that the orientation effects could be very important also at the stage of CN formation [34] (especially in the synthesis of SH nuclei [10]) by significantly decreasing the fusion probability for the nose-to-nose configurations which lead the nuclear system preferably into the QF channels. Up to now this effect was not taken into account explicitly in theoretical models; only the empirical parametrization of it had been used [27]. The main difficulty here is a calculation of the adiabatic potential energy for (in principle, unknown) subsequent shapes of the nuclear system starting from the configuration of arbitrary oriented two touching deformed nuclei and up to more or less spherical CN. Moreover, additional degrees of freedom are definitely needed to describe these complicated shapes. The standard two-centre shell model, as well as other macro–microscopic models, deals only with axially symmetric shapes.

Within the two-core model, we may calculate the adiabatic potential energy not only for axially symmetric shapes but also for the side-by-side initial orientation assuming that on the way to CN only the equatorial dynamic deformations of both fragments may change, whereas the static deformations of the cores (along axes perpendicular to the line connecting two centres) gradually relax to zero values with increasing equatorial deformation and mass transfer, see schematic figure 3. This assumption seems quite reasonable because there are no forces which may change the 'perpendicular' deformations of the fragments. In that case we need no additional degrees of freedom. The same variables β_1 and β_2 may be used for dynamic deformations along the axis between nuclear centres ($\beta_{1,2} = 0$ at contact). We assume that the static deformations of the nuclei just gradually disappear with increasing mass transfer and dynamic equatorial deformations: $\beta^{\perp}_{1,2} = \beta^{\perp}_{1,2}(0) \cdot \exp\left[-\left(\frac{\eta-\eta_0}{\Delta_\eta}\right)^2\right] \cdot \exp\left[-\left(\frac{\beta_{1,2}}{\Delta_\beta}\right)^2\right]$. Thus, they are not independent variables. Here η_0 is the initial mass asymmetry, $\beta^{\perp}_{1,2}(0)$ are the static deformations of the projectile and target, and $\Delta_\eta \sim \frac{10}{A_{\rm CN}}$ and $\Delta_\beta \sim 0.2$ are the adjusted parameters which do not much influence the whole dynamics.

The calculated driving potentials for the two fixed orientations of statically deformed ^{248}Cm nucleus fusing with ^{48}Ca are shown in figure 4 in the space of mass asymmetry and elongation. For the side collision the Coulomb barrier in the entrance channel is significantly higher. However, at the contact point this configuration is much more compact and the path to formation of CN is much shorter comparing with the tip (nose-to-nose) collisions. So we may expect higher fusion probability in this case, and our calculations (see below) confirm that. It is rather difficult (if possible, at all) to derive adiabatic potential energy of the nuclear system evolving from the configuration of arbitrary oriented touching deformed nuclei. In contrast, the diabatic potential energy is calculated easily in that case by using the double folding procedure, for example. To take somehow into account the orientation effect in the cross section of CN formation, we may simply average the results obtained for the two limiting orientations.

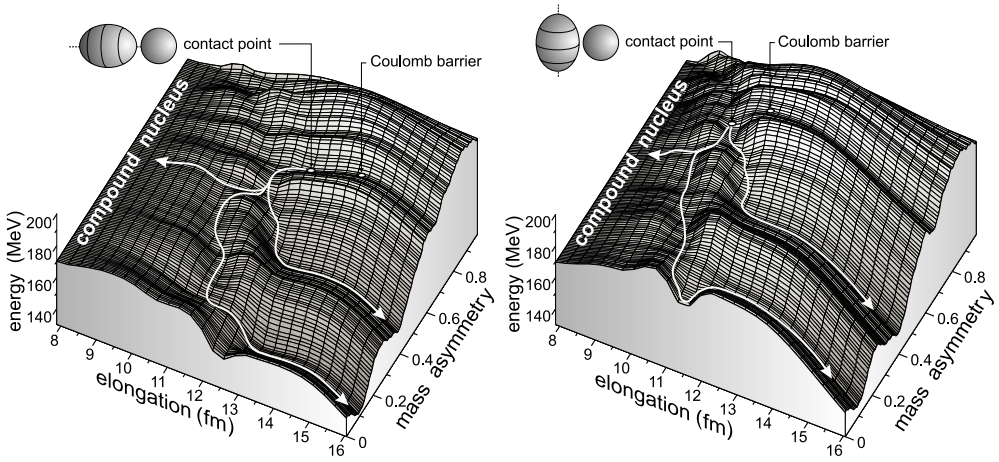

Figure 4. Driving potentials for the nuclear system formed in ^{48}Ca+^{248}Cm collision at tip (left) and side (right) orientations of statically deformed ^{248}Cm. The solid lines with arrows show schematically (without fluctuations) the projections of the QF trajectories (going to lead and tin valleys) and the path leading to formation of CN. The Coulomb barriers and the contact points are also marked for both cases.

2.2. Equations of motion

A choice of dynamic equations for the considered degrees of freedom is also not so evident. The main problem here is a proper description of nucleon transfer and change of the mass asymmetry which is a discrete variable by its nature. Moreover, the corresponding inertia parameter μ_η, being calculated within the Werner–Wheeler approach [35], becomes infinite at contact (scission) point and for separated nuclei. In [15], the inertialess Langevin-type equation for the mass asymmetry

$$\frac{\mathrm{d}\eta}{\mathrm{d}t} = \frac{2}{A_{\mathrm{CN}}} D_A^{(1)}(\eta) + \frac{2}{A_{\mathrm{CN}}} \sqrt{D_A^{(2)}(\eta)}\,\Gamma(t) \tag{1}$$

has been derived from the corresponding master equation for the distribution function $\varphi(A, t)$ [36, 37]. Here $\Gamma(t)$ is the normalized random variable with Gaussian distribution, $\langle\Gamma(t)\rangle = 0$, $\langle\Gamma(t)\Gamma(t')\rangle = 2\delta(t - t')$ and $D_A^{(1)}$, $D_A^{(2)}$ are the transport coefficients. A is the number of nucleons in one of the fragments and $\eta = (2A - A_{\mathrm{CN}})/A_{\mathrm{CN}}$.

Assuming that sequential nucleon transfers play a main role in mass rearrangement, i.e. $A' = A \pm 1$, we have

$$\begin{aligned} D_A^{(1)} &= \lambda(A \to A+1) - \lambda(A \to A-1) \\ D_A^{(2)} &= \tfrac{1}{2}[\lambda(A \to A+1) + \lambda(A \to A-1)]. \end{aligned} \tag{2}$$

For nuclei in contact the macroscopic transition probability $\lambda(A \to A' = A \pm 1)$ is defined by nuclear level density [36, 37] $\lambda^{(\pm)} = \lambda_0 \sqrt{\rho(A \pm 1)/\rho(A)} \approx \lambda_0 \exp\left(\frac{V(R,\beta,A\pm1) - V(R,\beta,A)}{2T}\right)$. Here $T = \sqrt{E^*/a}$ is the local nuclear temperature, $E^*(R, \beta, \eta)$ is the excitation energy, a is the level density parameter and λ_0 is the nucleon transfer rate ($\sim 10^{22}$ s^{-1} [36, 37]), which may, in principle, depend on excitation energy (the same holds for the diffuseness coefficient $D_A^{(2)}$). This feature, however, is not completely clear. In [36], the mass diffusion coefficient was assumed to be independent of excitation energy, whereas the microscopic consideration yields a square root dependance of it on nuclear temperature [38]. A linear dependence of the

mass diffusion coefficient on T was also used [39]. Here we treat the nucleon transfer rate λ_0 as a parameter of the model. Later we hope to derive the temperature dependence of this parameter from a systematic analysis of available experimental data.

Nucleon transfer for slightly separated nuclei is also rather probable. This intermediate nucleon exchange plays an important role in sub-barrier fusion processes [40] and has to be taken into account in equation (1). It can be done by using the following final expression for the transition probability:

$$\lambda^{(\pm)} = \lambda_0 \sqrt{\frac{\rho(A \pm 1)}{\rho(A)}}\, P_{\rm tr}(R, \beta, A \to A \pm 1). \tag{3}$$

Here $P_{\rm tr}(R, \beta, A \to A \pm 1)$ is the probability of one nucleon transfer depending on the distance between the nuclear surfaces. This probability goes exponentially to zero at $R \to \infty$, and it is equal to unity for overlapping nuclei. In our calculations, we used the semiclassical approximation for $P_{\rm tr}$ proposed in [40]. Equation (1) along with (3) defines a continuous change of mass asymmetry in the whole space (obviously, $\frac{{\rm d}\eta}{{\rm d}t} \to 0$ for far separated nuclei).

Finally, we have a set of 13 coupled Langevin-type equations (4) for seven degrees of freedom $\{R, \vartheta, \beta_1, \beta_2, \varphi_1, \varphi_2, \eta\} \equiv \vec{x}$ as shown in figure 1:

$$\begin{aligned}
&\frac{{\rm d}R}{{\rm d}t} = \frac{p_R}{\mu_R} \qquad \frac{{\rm d}\vartheta}{{\rm d}t} = \frac{\hbar\ell}{\mu_R R^2} \qquad \frac{{\rm d}\varphi_1}{{\rm d}t} = \frac{\hbar L_1}{\Im_1} \qquad \frac{{\rm d}\varphi_2}{{\rm d}t} = \frac{\hbar L_2}{\Im_2} \qquad \frac{{\rm d}\beta_1}{{\rm d}t} = \frac{p_{\beta_1}}{\mu_{\beta_1}} \\
&\frac{{\rm d}\beta_2}{{\rm d}t} = \frac{p_{\beta_2}}{\mu_{\beta_2}} \qquad \frac{{\rm d}\eta}{{\rm d}t} = \frac{2}{A_{\rm CN}} D_A^{(1)}(\eta) + \frac{2}{A_{\rm CN}} \sqrt{D_A^{(2)}(\eta)}\,\Gamma_\eta(t) \\
&\frac{{\rm d}p_R}{{\rm d}t} = -\frac{\partial V}{\partial R} + \frac{\hbar^2\ell^2}{\mu_R R^3} + \left(\frac{\hbar^2\ell^2}{2\mu_R^2 R^2} + \frac{p_R^2}{2\mu_R^2}\right)\frac{\partial \mu_R}{\partial R} + \frac{p_{\beta_1}^2}{2\mu_{\beta_1}^2}\frac{\partial \mu_{\beta_1}}{\partial R} + \frac{p_{\beta_2}^2}{2\mu_{\beta_2}^2}\frac{\partial \mu_{\beta_2}}{\partial R} \\
&\qquad\qquad - \gamma_R \frac{p_R}{\mu_R} + \sqrt{\gamma_R T}\,\Gamma_R(t) \\
&\frac{{\rm d}\ell}{{\rm d}t} = -\frac{1}{\hbar}\frac{\partial V}{\partial \vartheta} - \gamma_{\rm tang}\left(\frac{\ell}{\mu_R R} - \frac{L_1}{\Im_1}a_1 - \frac{L_2}{\Im_2}a_2\right) R + \frac{R}{\hbar}\sqrt{\gamma_{\rm tang} T}\,\Gamma_{\rm tang}(t) \\
&\frac{{\rm d}L_1}{{\rm d}t} = -\frac{1}{\hbar}\frac{\partial V}{\partial \varphi_1} + \gamma_{\rm tang}\left(\frac{\ell}{\mu_R R} - \frac{L_1}{\Im_1}a_1 - \frac{L_2}{\Im_2}a_2\right) a_1 - \frac{a_1}{\hbar}\sqrt{\gamma_{\rm tang} T}\,\Gamma_{\rm tang}(t) \\
&\frac{{\rm d}L_2}{{\rm d}t} = -\frac{1}{\hbar}\frac{\partial V}{\partial \varphi_2} + \gamma_{\rm tang}\left(\frac{\ell}{\mu_R R} - \frac{L_1}{\Im_1}a_1 - \frac{L_2}{\Im_2}a_2\right) a_2 - \frac{a_2}{\hbar}\sqrt{\gamma_{\rm tang} T}\,\Gamma_{\rm tang}(t) \\
&\frac{{\rm d}p_{\beta_1}}{{\rm d}t} = -\frac{\partial V}{\partial \beta_1} + \frac{p_{\beta_1}^2}{2\mu_{\beta_1}^2}\frac{\partial \mu_{\beta_1}}{\partial \beta_1} + \frac{p_{\beta_2}^2}{2\mu_{\beta_2}^2}\frac{\partial \mu_{\beta_2}}{\partial \beta_1} + \frac{\hbar^2 L_1^2}{2\Im_1^2}\frac{\partial \Im_1}{\partial \beta_1} + \left(\frac{\hbar^2\ell^2}{2\mu_R^2 R^2} + \frac{p_R^2}{2\mu_R^2}\right)\frac{\partial \mu_R}{\partial \beta_1} \\
&\qquad\qquad - \gamma_{\beta_1}\frac{p_{\beta_1}}{\mu_{\beta_1}} + \sqrt{\gamma_{\beta_1} T}\,\Gamma_{\beta_1}(t) \\
&\frac{{\rm d}p_{\beta_2}}{{\rm d}t} = -\frac{\partial V}{\partial \beta_2} + \frac{p_{\beta_1}^2}{2\mu_{\beta_1}^2}\frac{\partial \mu_{\beta_1}}{\partial \beta_2} + \frac{p_{\beta_2}^2}{2\mu_{\beta_2}^2}\frac{\partial \mu_{\beta_2}}{\partial \beta_2} + \frac{\hbar^2 L_2^2}{2\Im_2^2}\frac{\partial \Im_2}{\partial \beta_2} + \left(\frac{\hbar^2\ell^2}{2\mu_R^2 R^2} + \frac{p_R^2}{2\mu_R^2}\right)\frac{\partial \mu_R}{\partial \beta_2} \\
&\qquad\qquad - \gamma_{\beta_2}\frac{p_{\beta_2}}{\mu_{\beta_2}} + \sqrt{\gamma_{\beta_2} T}\,\Gamma_{\beta_2}(t).
\end{aligned} \tag{4}$$

Here φ_1 and φ_2 are the angles of rotation of the nuclei in reaction plane (their moments of inertia are $\Im_{1,2}(\beta_{1,2}) = k\frac{2}{5}M_{1,2}{R^0_{1,2}}^2 \cdot (1+\beta_{1,2}/3)$, $k \approx 0.4$), $a_{1,2} = R/2 \pm (R_1 - R_2)/2$ are the distances from the centres of the fragments up to the middle point between nuclear surfaces and $R_{1,2} = R^0_{1,2}[1 + \sqrt{5/4\pi}\beta_{1,2}P_2(\cos\vartheta)]$ are the nuclear radii. γ_R, $\gamma_{\rm tang}$ and $\gamma_{\beta_{1,2}}$ are the friction forces which depend generally on the coordinates $\vec{x}$. For the moment we ignore the non-diagonal terms of the mass and friction parameters. The so-called 'sliding friction' (which is proportional to the relative velocity of nearest nuclear surfaces $v_{\rm tang} = \frac{\hbar\ell}{\mu_R R} - \frac{\hbar L_1}{\Im_1}a_1 - \frac{\hbar L_2}{\Im_2}a_2$)

is mainly responsible for the dissipation of the angular momentum (see, e.g. [19, p. 265] and [41]). In our model the nucleus–nucleus potential energy depends on the distance between nuclear surfaces $\xi = R - R_{\rm contact}$, where $R_{\rm contact} = R_1(\eta, \beta_1, \varphi_1 - \vartheta) + R_2(\eta, \beta_2, \varphi_2 - \vartheta)$ (see figure 1). Therefore $\frac{\partial V}{\partial \varphi_1} + \frac{\partial V}{\partial \varphi_2} = -\frac{\partial V}{\partial \vartheta}$ and, thus, the total angular momentum $\ell + L_1 + L_2$ is conserved. Obviously, there is no dependence on φ_i if the ith nucleus is spherical.

Note that at near-barrier energies we are interested mainly in head-on collisions in which the nuclei may come in contact. Rotation of heavy nuclei (appearing at $L_{1,2} \neq 0$) is rather slow here and orientation effects manifest themselves mainly due to *initial* orientations of statically deformed nuclei. As mentioned above we calculate adiabatic potential energy surface only for the two limiting orientations (see figure 4), for which we solve numerically equations (4) assuming $\frac{\partial V}{\partial \varphi_1} = \frac{\partial V}{\partial \varphi_2} = 0$.

In our first calculations, we restricted ourselves to the consideration of only one spheroidal dynamic deformation variable β instead of independent deformations β_1 and β_2 of two fragments. We assumed 'equality of forces', i.e., $C_1\beta_1 = C_2\beta_2$, where $C_{1,2}$ are the LDM stiffness parameters of the fragments [41]. Using this ratio and $\beta_1 + \beta_2 = 2\beta$ the deformations of the fragments are derived from the common variable β.

2.3. Friction forces and nuclear viscosity

A number of different mechanisms have been suggested in the literature for being responsible for the energy loss in DI collisions. A discussion of the subject and appropriate references can be found, e.g., in [19]. The uncertainty in the strength of nuclear friction and in its form-factor is still large [42]. Because of that and for the sake of simplicity, we use here, for separated nuclei, the phenomenological nuclear friction forces with the Woods–Saxon radial form-factor $F(\zeta) = (1 + {\rm e}^{\zeta})^{-1}$, $\zeta = (\xi - \rho_F)/a_F$ and ξ is the distance between nuclear surfaces (see figure 1). The shift $\rho_F \sim 2$ fm serves to approach the position of the friction shape function to the strong absorption distance which is normally larger than the contact distance $R_{\rm contact}$ [43]. Thus $\gamma_R^F = \gamma_R^0 F(\xi - \rho_F)$, $\gamma_{\rm tang}^F = \gamma_t^0 F(\xi - \rho_F)$ and γ_R^0, γ_t^0, ρ_F and $a_F \sim 0.6$ fm are the model parameters.

For overlapping nuclei (mono-nucleus configuration) the two-body nuclear friction can be calculated within the Werner–Wheeler approach [35]. The corresponding viscosity coefficient μ_0 is however rather uncertain. From the analysis of fission-fragment kinetic energies it has been estimated to be of the order of several units of 10^{-23} Mev s fm^{-3} [35, 44]. The one-body dissipation mechanism [45, 46] leads in general to stronger nuclear friction, and some reduction coefficient for it is often used in specific calculations. Taking into account this uncertainty, we use here the Werner–Wheeler approach [35] for calculating the form-factors of nuclear friction $\gamma_R^{WW}(R, \beta_1, \beta_2, \eta)$ and $\gamma_{\beta_1,\beta_2}^{WW}(R, \beta_1, \beta_2, \eta)$ with the viscosity coefficient μ_0 which is treated as a model parameter. To keep continuity of kinetic energy dissipation at contact point, where two colliding nuclei form a mono-nucleus, we switched the phenomenological friction γ_R^F to γ_R^{WW} by the 'smoothed' (over 0.6 fm) step function $\theta_s(\xi) = (1 - {\rm e}^{-\xi/0.3})^{-1}$. There is no problem with the continuity at contact point for the nuclear friction γ_{β_1,β_2} associated with the surface deformations.

The two strength parameters of nuclear friction, γ_R^0 for well-separated nuclei and μ_0 for nuclear viscosity of the deformable mono-nucleus, reflect, from the one side, a possible difference in the mechanisms of dissipation of relative motion kinetic energy in DI collisions of two separated nuclei and nuclear viscosity of a mono-nucleus due to the coupling of collective motion (shape parameters) with the particle-hole excitations. On the other side, these friction strength parameters are of the same order of magnitude. Using $\mu_0 = 0.2 \times 10^{-22}$ MeV s fm^{-3} as proposed in [44], we get the nuclear friction $\gamma_R(\beta = 0) = 4\pi R_0 \mu_0 \approx 15$ MeV s fm^{-2}

for a change in elongation of a spherical nucleus with radius $R_0 = 6$ fm. This value can be compared with the value of nuclear friction of two nuclei in contact $\gamma_R(\xi = 0) = 13$ MeV s fm^{-2} estimated from the 'proximity theorem' ([19, p 269]). Nevertheless, as mentioned above, the uncertainty in the values of both parameters is very large [42]. Moreover, microscopic analysis shows that nuclear viscosity may also depend strongly on nuclear temperature [47]. Analysing experimental data on DI scattering of heavy ions we prefer to treat nuclear friction on phenomenological base using appropriate strength parameters γ_R^0 and μ_0, which later could be compared with those calculated microscopically [47].

2.4. Decay of primary fragments and cross sections

The cross sections for all the processes can be calculated in a simple and natural way. A large number of events (trajectories) are tested for a given impact parameter. Those events, in which the nuclear system overcame the fission barrier from the outside and entered the region of small deformations and elongations, are treated as fusion (CN formation). The other events correspond to quasi-elastic, DI and QF processes. Subsequent decay of the excited CN ($C \to B + xn + N\gamma$) is described then within the statistical model using an explicit expression for survival probability, which directly takes into account the Maxwell–Boltzmann energy distribution of evaporated neutrons

$$P_{ER}^{xn} = \int_0^{E_0^* - E_n^{\rm sep}(1)} \frac{\Gamma_n}{\Gamma_{\rm tot}}(E_0^*, J_0) P_n(E_0^*, e_1)\,{\rm d}e_1 \times \int_0^{E_1^* - E_n^{\rm sep}(2)} \frac{\Gamma_n}{\Gamma_{\rm tot}}(E_1^*, J_1) P_n(E_1^*, e_2)\,{\rm d}e_2 \cdots \times \int_0^{E_{x-1}^* - E_n^{\rm sep}(x)} \frac{\Gamma_n}{\Gamma_{\rm tot}}(E_{x-1}^*, J_{x-1}) P_n(E_{x-1}^*, e_x) \cdot G_{N\gamma}(E_x^*, J_x \to {\rm g.s.})\,{\rm d}e_x. \quad (5)$$

Here $E_n^{\rm sep}(k)$ and e_k are the binding and kinetic energies of the kth evaporated neutron, $E_k^* = E_0^* - \sum_{i=1}^{k} \left[E_n^{\rm sep}(i) + e_i\right]$ is the excitation energy of the residual nucleus after the emission of k neutrons, $P_n(E^*, e) = C\sqrt{e}\exp(-e/T(E^*))$ is the probability for the evaporated neutron to have energy e, and the normalization coefficient C is determined from the condition $\int_0^{E^* - E_n^{\rm sep}} P_n(E^*, e)\,{\rm d}e = 1$. The quantity $G_{N\gamma}$ defines the probability that the remaining excitation energy and angular momentum will be taken away by γ-emission after the evaporation of x neutrons. It can be approximated by the expression

$$G_{Ny}(E^*, J \to {\rm g.s.}) = \prod_{i=1}^{N} \frac{\Gamma_\gamma(E_i^*, J_i)}{\Gamma_{\rm tot}(E_i^*, J_i)}, \quad (6)$$

where $E_i^* = E^* - (i-1)\langle e_\gamma \rangle$, $J_i = J - (i-1)$, $\langle e_\gamma \rangle$ is the average energy of a dipole γ-quantum, and the number of γ-quanta N is determined from the condition $E_N^* < B_{\rm fis}$, assuming that at energies lower than the fission barrier the fission probability is very small as compared to γ-emission. All the corresponding widths, $\Gamma_n, \Gamma_p, \Gamma_\gamma$ and $\Gamma_{\rm fis}$, have been calculated in accordance with [48].

The double differential cross-sections of all the processes are calculated as follows:

$$\frac{{\rm d}^2\sigma_\eta}{{\rm d}\Omega\,{\rm d}E}(E, \theta) = \int_0^\infty b\,{\rm d}b \frac{\Delta N_\eta(b, E, \theta)}{N_{\rm tot}(b)} \frac{1}{\sin(\theta)\Delta\theta\Delta E}. \quad (7)$$

Here $\Delta N_\eta(b, E, \theta)$ is the number of events at a given impact parameter b in which the system enters into the channel η (definite mass asymmetry value) with kinetic energy in the region $(E, E + \Delta E)$ and centre-of-mass outgoing angle in the region $(\theta, \theta + \Delta\theta)$, $N_{\rm tot}(b)$ is the total

number of simulated events for a given value of impact parameter. In collisions of deformed nuclei averaging over initial orientations should be performed. It is made quite simply for DI and capture cross sections because the diabatic potential energy surface is easily calculated for any orientation of deformed nuclei. Probability of CN formation is determined mainly by the adiabatic potential, which, as mentioned above, can be calculated for the moment only for the two limiting orientations of touching deformed nuclei. Thus, the cross section of CN formation was calculated by averaging the results obtained for these two limiting orientations (nose-to-nose and side-by-side).

Expression (7) describes the mass, energy and angular distributions of the *primary* fragments formed in the binary reaction (both in DI and in QF processes). Subsequent de-excitation cascades of these fragments via fission and emission of light particles and gamma-rays were taken into account explicitly for each event within the statistical model leading to the *final* mass and energy distributions of the reaction fragments. The sharing of the excitation energy between the primary fragments was assumed to be proportional to their masses. For each excited fragment the multi-step decay cascade was analysed taking into account a competition between evaporation of neutrons and/or protons and fission. At the final stage of the evaporation cascade $\left(E^* < E_n^{\rm sep}\right)$ a competition between γ-emission and fission was taken into account in the same way as for survival of CN (see above). Due to rather high excitations of the fragments the analysis of this evaporation cascade needs the longest computation time. Mass, energy and angular distributions of the fission fragments (regular fission of CN) are also estimated within the statistical model using the dependent on the mass asymmetry adiabatic potential energy surface at the scission point. Use of the statistical model at the last reaction stage (for estimation of survivability of CN and/or decay of highly excited primary reaction fragments) allows one to estimate the cross sections up to 1 pb or less, i.e. up to the probabilities of 10^{-12}.

Neutron emission during a long evolution of the system going into the QF channels or CN formation was also taken into account. However, it was found that pre-scission and pre-compound neutron evaporation does not influence significantly the gross properties of DI and QF processes (see below).

The used model allows us to perform also a time analysis of the studied reactions. Each tested event is characterized by the reaction time $\tau_{\rm int}$, which is calculated as a difference between re-separation (scission) and contact times. Those events, in which nuclei do not come in contact (e.g., for large impact parameters), are excluded from the analysis. In such a way, for all the channels we may calculate and analyse reaction time distributions and the corresponding cross sections $\mathrm{d}\sigma_\eta/\mathrm{d}\tau_{\rm int}$.

3. Deep inelastic scattering and quasi-fission processes

At first we applied the model to describe available experimental data on low-energy damped collision of very heavy nuclei, ^{136}Xe+^{209}Bi [49], where the DI process should dominate due to expected prevalence of the Coulomb repulsion over nuclear attraction and the impossibility of CN formation. The adiabatic potential energy surface of this nuclear system is shown in figure 5 in the space of elongation and mass asymmetry at fixed zero deformations. The colliding nuclei are very compact with almost closed shells, and the potential energy has only one deep valley corresponding to the entrance channel ($\eta \sim 0.21$) giving rather simple mass distribution of the reaction fragments. In that case, the reaction mechanism should depend mainly on the nucleus–nucleus potential at contact distance (which determines the grazing angle), on the friction forces at this region (which determine the energy loss) and on nucleon transfer rate at contact. Note that there is a well-pronounced plateau at contact configuration

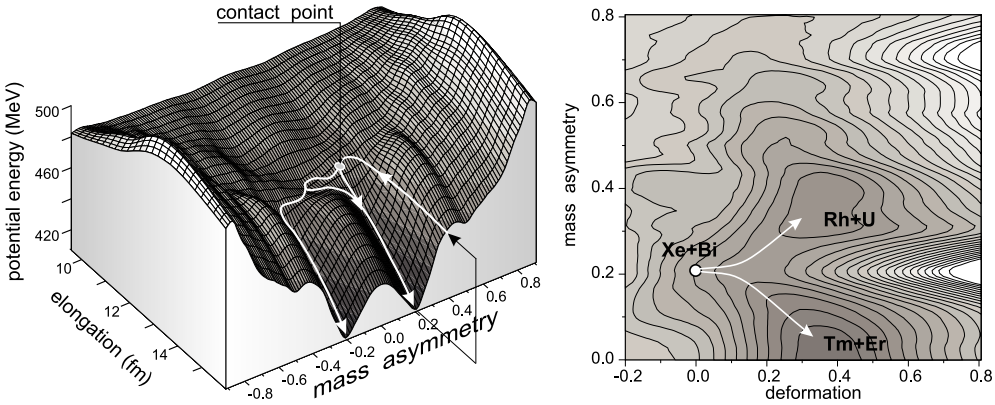

Figure 5. Driving potential for the nuclear system formed in ^{136}Xe+^{209}Bi collision at fixed deformations (left) and at contact configuration (right). The solid lines with arrows show schematically (without fluctuations) most probable trajectories.

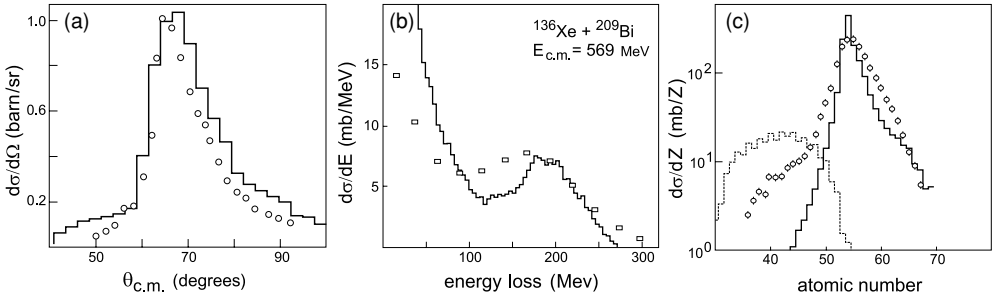

Figure 6. Angular (a), energy-loss (b) and charge (c) distributions of the Xe-like fragments obtained in the ^{136}Xe+^{209}Bi reaction at $E_{\text{c.m.}} = 568$ MeV. Experimental data are taken from [49]. Histograms are the theoretical predictions. The low-Z wing of the experimental charge distribution is due to incompletely removed events of sequential fission of the heavy fragment [49]. Dotted histogram in (c) indicates the calculated total yield of sequential fission fragments.

in the region of zero mass asymmetry (see figure 5). It becomes even lower with increasing the deformations and corresponds to the formation of the nuclear system consisting of strongly deformed touching fragments ^{172}Er+^{173}Tm (see right panel of figure 5), which means that a significant mass rearrangement may occur here leading to additional time delay of the reaction.

On the right panel of figure 5 the landscape of the potential energy is shown at contact configuration depending on mass asymmetry and deformation of the fragments. As can be seen, after contact and before re-separation the nuclei aim to become more deformed. Moreover, beside a regular diffusion (caused by the fluctuations), the final mass distribution is determined also by the two well-marked driving paths leading the system to more and to less symmetric configurations. They are not identical and this leads to the asymmetric mass distribution of the primary fragments, see figure 6(c). This effect may be interpreted as a week manifestation of the OF processes when the mass distribution is not determined only by a simple diffusion process but also by the shell structure of nuclear system.

In spite of a short penetration of nuclei into each other, the reaction cross sections were found to be sensitive to the value of nuclear viscosity of the mono-nucleus, μ_0, mainly

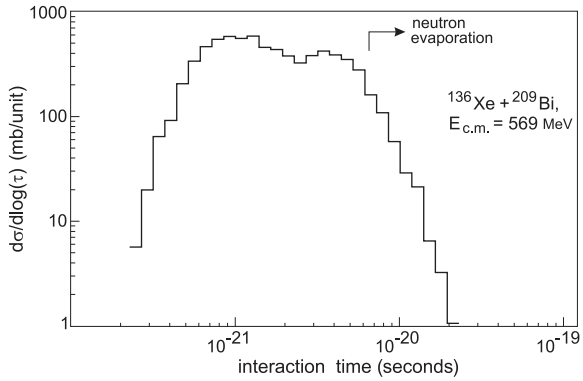

Figure 7. Reaction time distribution for the ^{136}Xe+^{209}Bi collision at 569 MeV centre-of-mass energy.

due to the large dynamic deformations of the reaction fragments. The value of $\mu_0 = 1 \times 10^{-22}$ Mev s fm^{-3} has been used to describe properly the reaction cross sections at the centre-of-mass beam energy of 568 MeV. This value is larger than those found for low-excited fissile nuclei [44], which evidently indicates on a temperature dependence of the nuclear viscosity [47]. The values of other friction parameters have been taken from [15]. The nucleon transfer rate was fixed at $\lambda_0 = 0.05 \times 10^{22}$ s^{-1}. This rather small value was found to be sufficient to reproduce the mass distributions of reaction products mainly due to additional driving to more and to less mass asymmetry with increasing deformation (see right panel of figure 5).

In figure 6, the angular, energy and charge distributions of the Xe-like fragments are shown comparing with our calculations (histograms). In accordance with experimental conditions only the events with the total kinetic energy in the region of $260 \leqslant E \leqslant 546$ MeV and with the scattering angles in the region of $40^\circ \leqslant \theta_{\mathrm{c.m.}} \leqslant 100^\circ$ were accumulated. The total cross section corresponding to all these events is about 2200 mb (experimental estimation is 2100 mb [49]). Due to the rather high excitation energy sequential fission of the primary heavy fragments may occur in this reaction (mainly those heavier than Bi). In the experiment the yield of the heavy fragments was found to be about 30% less comparing with Xe-like fragments. Our calculation gives 354 mb for the cross section of sequential fission, which is quite comparable with experimental data. Mass distribution of the fission fragments is shown in figure 6(c) by the dotted histogram. Note that it is a contamination with sequential fission products of heavy primary fragments leading to the bump around $Z = 40$ in the experimental charge distribution in figure 6(c).

The interaction time is one of the most important characteristics of nuclear reactions, though it cannot be measured directly. The total reaction time distribution, $\frac{\mathrm{d}\sigma}{\mathrm{dlog}(\tau)}$ (τ denotes the time between the moments of contact of two nuclei and re-separation of the fragments), is shown in figure 7 for the studied reaction. In most of the damped collisions ($E_{\mathrm{loss}} > 35$ MeV) the interaction time is rather short ($\sim 10^{-21}$ s). These fast events correspond to collisions with intermediate impact parameters. Nevertheless, a large amount of kinetic energy is dissipated here very fast at relatively low mass transfer.

However, in some cases, in spite of an absence of attractive potential pocket the system may hold in contact rather long. During this time it moves over the multi-dimensional potential energy surface with almost zero kinetic energy (result of large nuclear viscosity) mainly in deformation and mass-asymmetry space (see right panel of figure 5). Note that it is the longest component of the time distribution (second peak in figure 7) which corresponds to the most

dissipative collisions. Large overlap of nuclear surfaces takes place here and, as a result, significant mass rearrangement may occur. In the TKE-mass plot, these events spread over a wide region of mass fragments (including symmetric splitting) with kinetic energies very close to kinetic energy of fission fragments (see pronounced bump and its tail in the energy-loss distribution in figure 6(b)). Some gap between the two groups in the energy and in the time distributions can also be seen in figures 6(b) and 7. All these make the second group of slow events quite distinguished from the first one. These events are more similar to fission than to deep-inelastic processes. Formally, they also can be marked as quasi-fission.

For the highly excited nuclear system neutron evaporation is possible before re-separation of the fragments. In figure 7, the arrow indicates the interaction time after which the probability of neutron emission becomes notable in the system ^{136}Xe+^{209}Bi at excitation energy of 100 MeV (reached at this moment of interaction time). However, the calculations show that only a few neutrons (about 1 on average) may evaporate at this intermediate reaction stage and this does not influence significantly the angular, energy and mass distributions of the reaction products. Nucleon evaporation from the excited primary fragments is very important in this reaction changing the mass and energy distributions of detected final reaction products.

Let us consider now the near-barrier ^{48}Ca+^{248}Cm fusion reaction (leading to the formation of a super-heavy nucleus) in which the QF process plays a dominant role. The potential energy surfaces for this nuclear system are shown in figure 4 for two different initial orientations of the ^{248}Cm nucleus at fixed dynamic deformation, which also plays a very important role here. Our calculations show that after overcoming the Coulomb barrier the fragments become first very deformed, then the mass asymmetry gradually decreases and the system finds itself in the quasi-fission valley with one of the fragments close to the doubly magic nucleus ^{208}Pb (see deep valley at $\eta \approx 0.4$ in figure 4). To simulate somehow the neck formation in the QF channels and to describe properly the energy distribution of reaction fragments, we assumed that the radial parameters of the formfactors of the friction forces are different in the entrance and exit channels. In the first case, the contact distance was calculated as $R_{\rm contact}(\eta, \beta) = [R_1(A_1, \beta_1) + R_2(A_2, \beta_2)]$ with $r_0 = 1.16$ fm, whereas for the QF channels the scission distance (up to which the friction forces keep on) was defined as $R_{\rm scission}(\eta, \beta) = (1.4/r_0)[R_1(A_1, \beta_1) + R_2(A_2, \beta_2)] + 1$ fm. The solid line in figure 8(b) just corresponds to the potential energy at the scission point $V(r = R_{\rm scission}, \beta, \eta) + Q_{gg}(\eta)$ minimized over β.

Figure 8 shows the experimental and calculated correlations of the total kinetic energy and the mass distributions of the primary reaction products along with inclusive mass distribution for the ^{48}Ca+^{248}Cm reaction at the near-barrier energy of $E_{\rm c.m.} = 203$ MeV. The tails of the DI component to the unphysical high energies (higher than $E_{\rm c.m.}$ at $A_1 \sim 50$ and $A_2 \sim 250$) and to very low energies with more symmetric mass combinations in figure 8(a) (absent in the calculations in figure 8(b)) are due to the specific experimental procedure [50]. The large yield of the fragments in the region of doubly magic nucleus ^{208}Pb (and the complimentary light fragments) is the most pronounced feature of the TKE-mass distribution. These QF process ('symmetrizing' quasi-fission) is the dominant channel in reactions of such kind which protects the nuclei from fusing (formation of compound nucleus).

The probability for CN formation in this reaction was found to be very small and depended greatly on the incident energy. Due to a strong dissipation of kinetic energy just the fluctuations (random forces) define the dynamics of the system after the contact of the two nuclei. At near-barrier collisions the excitation energy (temperature) of the system is rather low, the fluctuations are weak and the system chooses the most probable path to the exit channel along the quasi-fission valley (see figure 4). However, at non-zero excitation energy there is a chance for the nuclear system to overcome the multi-dimensional inner potential barriers and

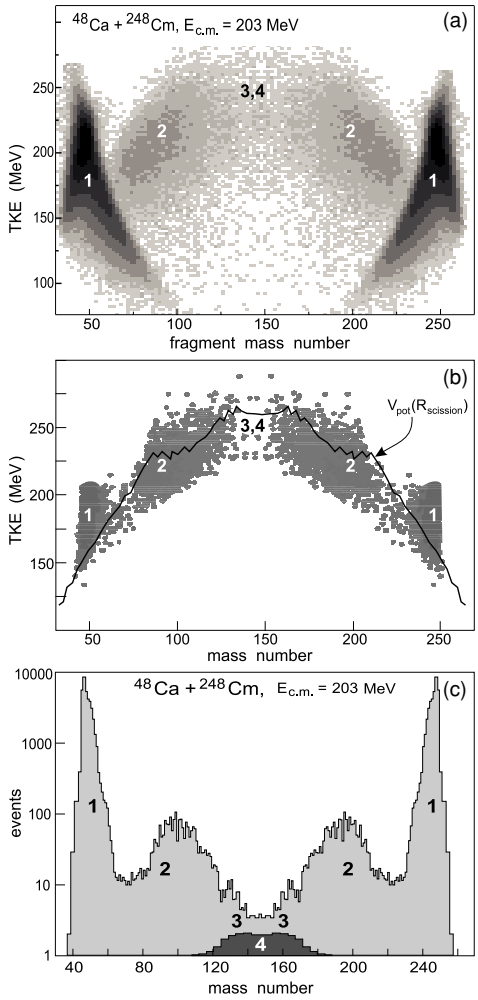

Figure 8. Experimental (a) and calculated (b) TKE-mass distributions of reaction products in collision of ^{48}Ca+^{248}Cm at $E_{\rm c.m.} = 203$ MeV. (c) Contributions of DI (1), QF (2,3) and fusion–fission (4) processes into inclusive mass distribution.

find itself in the region of the CN configuration (small deformation and elongation). Within the Langevin calculations a great number of events should be tested to find this low probability. For the studied reaction, for example, only several fusion events have been found among more than 10^5 total tested events (see dark region 4 in figure 8(c)).

The cross section of CN formation in these reactions was found really dependent on initial orientation of the statically deformed ^{248}Cm nucleus. Having for the moment the potential energy surface only for the two limiting orientations (see figure 4), we performed here a simple averaging of the cross sections obtained for the tip and side configurations. Due to a lower Coulomb barrier, the tip collisions lead to larger value of the capture cross section compared with the side collisions. If we define the capture cross section as all the events in which the nuclei overcome the Coulomb barrier, come in contact and fuse or re-separate with the mass rearrangement exceeding 20 mass units (to distinguish it somehow from the DI cross section), then $\sigma_{\rm cap} \approx 45$ mb for tip collisions and only 5 mb for the side ones at the beam energy of

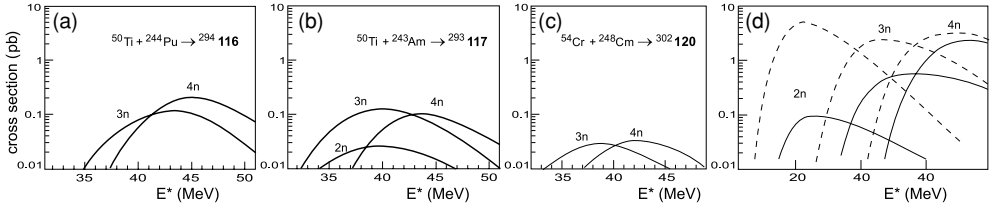

Figure 9. Evaporation residue cross sections for the fusion reactions ^{50}Ti+^{244}Pu (a), ^{50}Ti+^{243}Am (b), ^{54}Cr+^{248}Cm (c) and ^{136}Xe+^{136}Xe (d).

$E_{\text{c.m.}} = 203$ MeV. However, (unambiguously defined) fusion cross sections were found to be rather close for both cases (about 0.03 mb and 0.04 mb, respectively), which means that CN formation at this energy is about ten times more probable for the side-oriented touching nuclei. This result is in a reasonable agreement with those found previously [27] and with the yield of evaporation residues in this reaction [10].

Note that a direct experimental study of an influence of static deformations of heavy nuclei on a probability of CN formation could be done by comparison of the capture and evaporation residue cross sections for two fusion reactions, ^{64}Zn+^{150}Nd and ^{70}Zn+^{144}Nd, leading to the *same* compound nucleus ^{214}Th. In the first case the nuclei, ^{64}Zn and ^{150}N, have non-zero deformations in their ground states, whereas ^{70}Zn and ^{144}N are spherical nuclei. We may expect that the excitation functions for the yields of evaporation residues will be quite different for the two reactions reflecting an influence of the orientation effects on the fusion probability.

Within our approach, we estimated a possibility of SH element production in the asymmetric fusion reactions of nuclei heavier than ^{48}Ca with transuranium targets. Such reactions can be used, in principle, for a synthesis of the elements heavier than 118. Evaporation residue (EvR) cross sections for the fusion reactions ^{50}Ti+^{244}Pu, ^{50}Ti+^{243}Am and ^{54}Cr+^{248}Cm are shown in figure 9. For all cases we used the fission barriers of CN predicted by the macro–microscopical model [30], which gives much lower fission barrier for ^{302}120 nucleus in comparison with ^{296}116. However, full microscopic models based on the self-consistent Hartree–Fock calculations [51] predict much higher fission barriers for the nucleus ^{302}120 (up to 10 MeV for the Skyrme forces). This means that the 3n and 4n EvR cross sections in the ^{54}Cr+^{248}Cm fusion reactions could be two or three orders of magnitudes higher as compared with those shown in figure 9(c).

Another possibility for a synthesis of the neutron-rich SH elements beyond 118 is the fusion reactions of symmetric nuclei (fission-like fragments). However, in such reactions an uncertainty in the calculation of very small cross sections for CN formation is rather large. Dashed and solid curves in figure 9(d) reflect this uncertainty in our estimations of the EvR cross sections in ^{136}Xe+^{136}Xe fusion reactions. If the experiment (planned to be performed in Dubna) will give the EvR cross sections at the level of few picobarns for this reaction, then we may really dream about using neutron-rich accelerated fission fragments for the production of SH elements in the region of the 'island of stability' (e.g., ^{132}Sn+^{176}Yb→^{308}120). Detailed analysis of CN formation in 'cold' (more symmetric) and 'hot' (asymmetric) fusion reactions leading to the formation of super-heavy elements will be done separately.

4. Low-energy collisions of transactinide nuclei

Reasonable agreement of our calculations with experimental data on low-energy DI and QF reactions induced by heavy ions (see Section 3) stimulated us to study the reaction dynamics

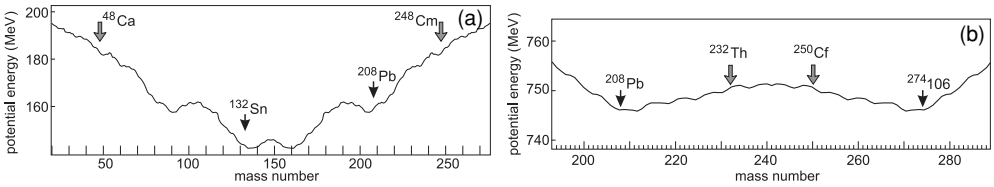

Figure 10. Potential energy at contact 'nose-to-nose' configuration for the two nuclear systems formed in ^{48}Ca+^{248}Cm (a) and ^{232}Th+^{250}Cf (b) collisions. Spheroidal deformation is equal 0.2 for both cases.

of very heavy transactinide nuclei. The purpose was to find an influence of the shell structure of the driving potential (in particular, deep valley caused by the double shell closure $Z = 82$ and $N = 126$) on nucleon rearrangement between primary fragments. First results of such calculations have been already published in [52]. In figure 10, the potential energies are shown depending on mass rearrangement at contact configuration of the nuclear systems formed in ^{48}Ca+^{248}Cm and ^{232}Th+^{250}Cf collisions. The lead valley evidently reveals itself in both cases (for ^{48}Ca+^{248}Cm system there is also a tin valley). In the first case (^{48}Ca+^{248}Cm), discharge of the system into the lead valley (normal or symmetrizing quasi-fission) is the main reaction channel, which decreases significantly the probability of CN formation. In collisions of heavy nuclei (Th+Cf, U+Cm and so on), we expect that the existence of this valley may notably increase the yield of surviving neutron-rich super-heavy nuclei complementary to the projectile-like fragments around ^{208}Pb ('inverse' or anti-symmetrizing quasi-fission process).

Direct time analysis of the reaction dynamics allows us to estimate also the lifetime of the composite system consisting of two touching heavy nuclei with total charge $Z > 180$. Such 'long-living' configurations may lead to spontaneous positron emission from super-strong electric field of giant quasi-atoms by a static QED process (transition from neutral to charged QED vacuum) [16, 17]. About twenty years ago an extended search for this fundamental process was carried out, and narrow line structures in the positron spectra were first reported at GSI. Unfortunately, these results were not confirmed later, neither at ANL [53], nor in the last experiments performed at GSI [54, 55] (see also hierarchical references therein). These negative findings, however, were contradicted by Jack Greenberg (private communication and supervised thesis at Wright Nuclear Structure Laboratory, Yale University). Thus the situation remains unclear, while the experimental efforts in this field have ended. We hope that new experiments and new analysis, performed according to the results of our dynamical model, may shed additional light on this problem and also answer the principal question: are there some reaction features (triggers) testifying a long reaction delays? If they are, new experiments should be planned to detect the spontaneous positrons in the specific reaction channels. As we know, such experiments are in progress [56].

Of course, for such heavy nuclei there is most likely no attractive potential pocket typical for lighter nuclear systems [57], the potential is repulsive everywhere. However, the potential energy is not very steep in the region of the contact point and two nuclei may keep in contact for a long time changing their deformations and transferring nucleons to each other. Projections of the multi-dimensional adiabatic potential energy surface onto the $R - \eta$ and $R - \beta$ planes are shown in figure 11 along with a typical 'trajectory' for the nuclear system formed in collision of ^{232}Th+^{250}Cf.

4.1. Primary fragments

Using the same parameters of nuclear viscosity and nucleon transfer rate as for the system Xe+Bi (see above), we calculated the yield of primary and surviving fragments formed in the

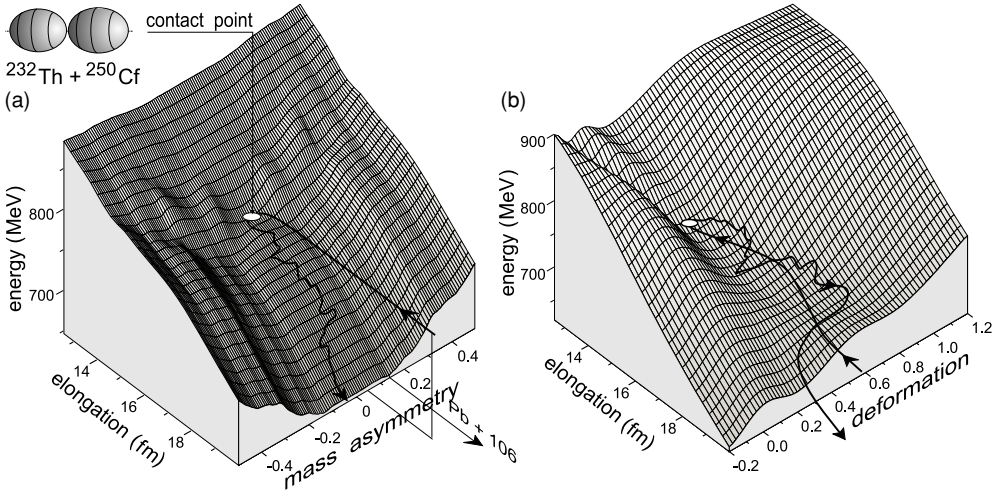

Figure 11. Potential energy surface for the nuclear system formed by ^{232}Th+^{250}Cf as a function of R and η ($\beta = 0.22$) (a), and R and β ($\eta = 0.037$) (b). A typical trajectories are shown by the thick curves with arrows. Before nuclei reach the region of nuclear friction forces, they are in their ground states (zero temperature) and no fluctuations occur. However when nuclei come in contact they are already well excited and fluctuations play a significant role.

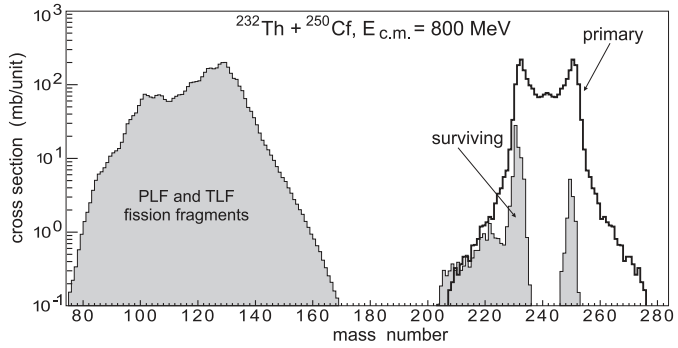

Figure 12. Mass distributions of primary (solid histogram), surviving and sequential fission fragments (hatched areas) in the ^{232}Th+^{250}Cf collision at 800 MeV centre-of-mass energy.

^{232}Th+^{250}Cf collision at 800 MeV centre-of-mass energy. Low fission barriers of the colliding nuclei and of the most of the reaction products jointly with rather high excitation energies of them in the exit channel will lead to very low yield of surviving heavy fragments. Indeed, sequential fission of the projectile-like and target-like fragments dominate in these collisions, see figure 12. At first sight, there is no chances to get surviving super-heavy nuclei in such reactions. However, as mentioned above, the yield of the primary fragments will increase due to the QF effect (lead valley) as compared to the gradual monotonic decrease typical for damped mass transfer reactions. Secondly, with increasing neutron number the fission barriers increase on average (also there is the closed sub-shell at $N = 162$). Thus we may expect a non-negligible yield (at the level of 1 pb) of surviving super-heavy neutron-rich nuclei produced in these reactions.

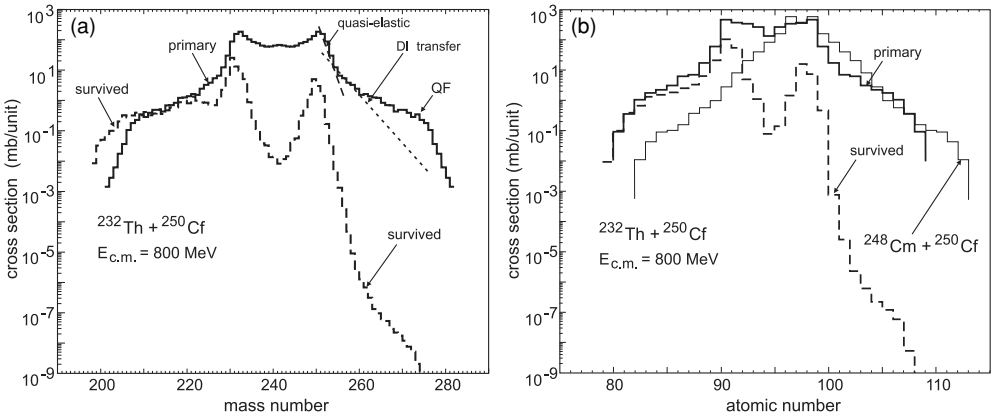

Figure 13. Mass (a) and charge (b) distributions of primary (solid histograms) and surviving (dashed histograms) fragments in the ^{232}Th+^{250}Cf collision at 800 MeV centre-of-mass energy. Thin solid histogram in (b) shows the primary fragment distribution in the hypothetical reaction ^{248}Cm+^{250}Cf.

4.2. SHE production

Results of much longer calculations are shown in figure 13, where the mass and charge distributions of surviving fragments obtained in the ^{232}Th+^{250}Cf collision at 800 MeV are presented. The pronounced shoulder can be seen in the mass distribution of the primary fragments near the mass number A=208. It is obviously explained by the existence of a notable valley in the potential energy surface (see figures 10(b) and 11(a)), which corresponds to the formation of doubly magic nucleus ^{208}Pb ($\eta = 0.137$). The emerging of the nuclear system into this valley resembles the well-known quasi-fission process and may be called 'inverse (or anti-symmetrizing) quasi-fission' (the final mass asymmetry is larger than the initial one). For $\eta > 0.137$ (one fragment becomes lighter than lead), the potential energy sharply increases and the mass distribution of the primary fragments decreases rapidly at $A < 208$ ($A > 274$). The same is true for the charge distribution at $Z < 82$ ($Z > 106$). As a result, in the charge distribution of the surviving heavy fragments, figure 13 (b), there is also a shoulder at $Z \sim 106$ and the yield of nuclei with $Z > 107$ was found in this reaction at the level of less than 1 pb. This result differs sharply from those obtained in [58], where the reactions of such kind have been analysed within the parametrized diffusion model, and the yield of heavy primary fragments was found to diminish monotonically with increasing charge number. The authors of [58] concluded, however, that the 'fluctuations and shell effects not taken into account may considerably increase the formation probabilities'. Such is indeed the case.

In figure 14, the available experimental data on the yield of SH nuclei in collisions of ^{238}U+^{238}U [3] and ^{238}U+^{248}Cm [5] are compared with our calculations performed at 800 MeV centre-of-mass energy. In these experiments thick targets have been used, which means that the experimental data were, in fact, integrated over the energy in the region of about 750–850 MeV [3, 5]. The estimated excitation functions for the yield of heavy surviving nuclei, shown in figure 15, demonstrate a rather strong dependence on beam energy, though not so sharp as in fusion reactions. In spite of that, the agreement of our calculations with experimental data is quite acceptable, worse for few-nucleon transfer but better for more dissipative and longer massive transfer processes, for which the model is more suitable.

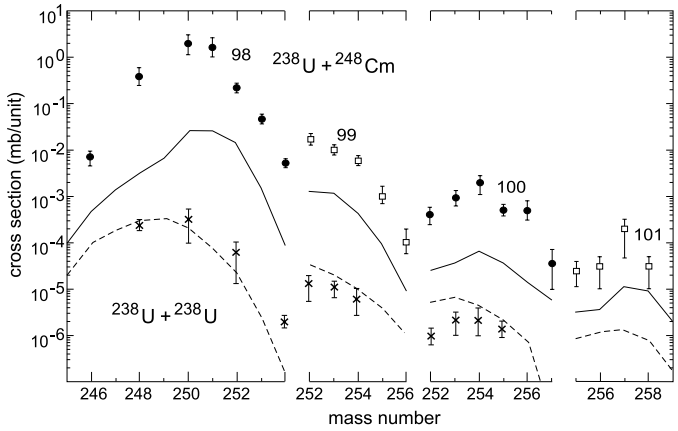

Figure 14. Isotopic yield of the elements 98–101 in the reactions ^{238}U+^{238}U (crosses) [3] and ^{238}U+^{248}Cm (circles and squares) [5]. The curves show the results of our calculations.

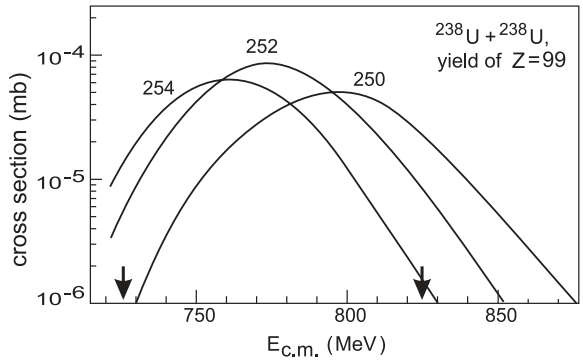

Figure 15. Excitation functions for the yields of Es isotopes (numbers near the curves) for the ^{238}U+^{238}U reactions. The arrows indicate potential energies of two colliding nuclei at contact ($r_0 = 1.16$ fm) for tip (left) and side (right) configurations.

The estimated isotopic yields of survived SH nuclei in the ^{232}Th+^{250}Cf, ^{238}U+^{238}U and ^{238}U+^{248}Cm collisions at 800 MeV centre-of-mass energy are shown in figure 16. Thus, as we can see, there is a real chance for producing the long-lived neutron-rich SH nuclei in such reactions. As the first step, chemical identification and study of the nuclei up to $^{274}_{107}$Bh produced in the reaction ^{232}Th+^{250}Cf may be performed. As can be seen from figures 15 and 16 the yield of SH elements in damped reactions with transactinides depends strongly on beam energy and on nuclear combination which should be chosen carefully. In particular, in figure 13 the estimated yield of the primary fragments obtained in the hypothetical reaction ^{248}Cm+^{250}Cf (both constituents are radioactive) is shown, demonstrating a possibility for production of SH neutron-rich nuclei up to the element 112 (complementary to lead fragments in this reaction).

4.3. Time analysis

The time analysis of the reactions studied shows that in spite of non-existing attractive potential pocket the system consisting of two very heavy nuclei may hold in contact rather long in some cases. During this time the giant nuclear system moves over the multi-dimensional potential

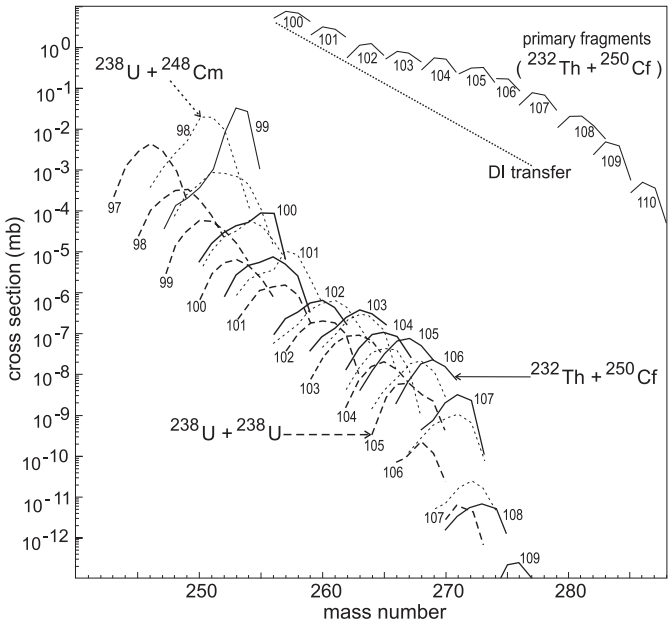

Figure 16. Yield of super-heavy nuclei in collisions of ^{238}U+^{238}U (dashed), ^{238}U+^{248}Cm (dotted) and ^{232}Th+^{250}Cf (solid lines) at 800 MeV centre-of-mass energy. Solid curves in upper part show isotopic distribution of primary fragments in the Th+Cf reaction. In the case of U+Cm the upper curve only is marked by Z-number ($Z = 98$), the others are one by one up to $Z = 107$.

energy surface with almost zero kinetic energy (result of large nuclear viscosity), a typical trajectory is shown in figure 11. The total reaction time distribution, $\frac{d\sigma}{d\log(\tau)}$ (τ denotes the time after the contact of two nuclei), is shown in figure 17 for the ^{238}U+^{248}Cm collision. We found that the dynamic deformations are mainly responsible here for the time delay of the nucleus–nucleus collision. Ignoring the dynamic deformations in the equations of motion significantly decreases the reaction time, see figure 17(a). With increase of the energy loss and mass transfer the reaction time becomes longer and its distribution becomes more narrow, see figure 17(b). Note that the lifetime of the nuclear system formed in Au+Au collision was estimated recently within the molecular dynamics model [59] and also found to be rather long, though at well above barrier energy.

As mentioned earlier, the lifetime of a giant composite system more than 10^{-20} s is quite enough to expect positron line structure emerging on top of the dynamical positron spectrum due to spontaneous e^+e^- production from the super-critical electric fields as a fundamental QED process ('decay of the vacuum') [16, 17]. The absolute cross section for long events ($\tau > 10^{-20}$ s) is found to be maximal just at the beam energy ensuring the two nuclei to be in contact, see figure 17(c). Note that the same energy is also optimal for the production of the most neutron-rich SH nuclei (figure 15). Of course, there are some uncertainties in the used parameters, mostly in the value of nuclear viscosity. However, we found only a linear dependence of the reaction time on the strength of nuclear viscosity, which means that the obtained reaction time distribution is rather reliable; see logarithmic scale on both axes in figure 17(a). Note also that the time distribution shown in figure 17 corresponds to the time intervals between contact and scission of reaction fragments. However, the electron eigenstates of the quasi-atom are weakly sensitive to a re-separation of nuclei (and depend on

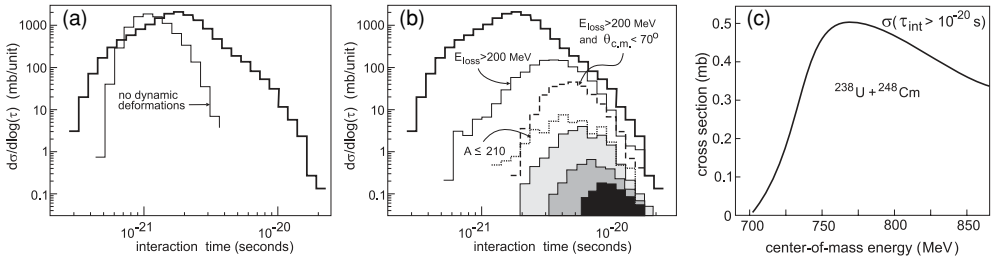

Figure 17. Reaction time distributions for the ^{238}U+^{248}Cm collision at 800 MeV centre-of-mass energy. Thick solid histograms correspond to all events with energy loss more than 30 MeV. (a) Thin solid histogram shows the effect of switching-off dynamic deformations. (b) Thin solid, dashed and dotted histograms show reaction time distributions in the channels with formation of primary fragments with $E_{loss} > 200$ MeV, $E_{loss} > 200$ MeV and $\theta_{c.m.} < 70^\circ$ and $A \leqslant 210$, correspondingly. Hatched areas show time distributions of events with formation of the primary fragments with $A \leqslant 220$ (light gray), $A \leqslant 210$ (gray), $A \leqslant 204$ (dark) having $E_{loss} > 200$ MeV and $\theta_{c.m.} < 70^\circ$. (c) Cross section for events with interaction time longer than 10^{-20} s depending on beam energy.

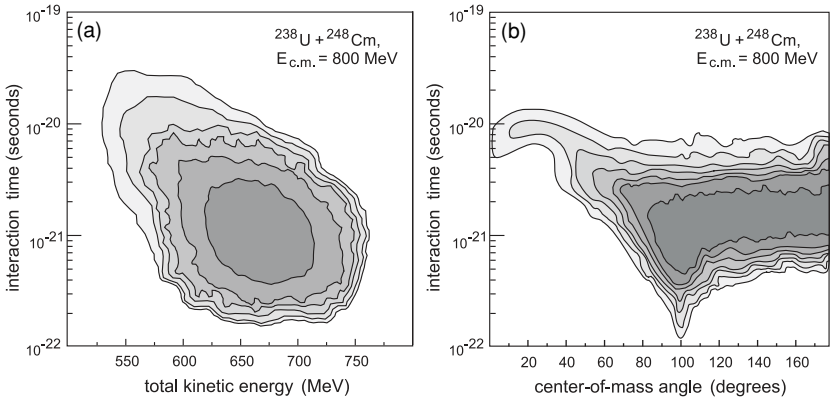

Figure 18. Energy-time (a) and angular-time (b) distributions of primary fragments in the ^{238}U+^{248}Cm collision at 800 MeV ($E_{loss} > 15$ MeV). Landscape is shown in logarithmic scale—lines are drawn over one order of magnitude. The quasi-elastic peak is removed.

the total charge $Z_1 + Z_2$) as long as the distance between nuclear centres is shorter than the electron Compton wavelength (validating the monopole approximation for the Dirac orbits, see [17]). Thus the lifetime distribution of giant quasi-atoms is even slightly wider than it is shown in figure 17(a).

Formation of the background positrons in these reactions forces one to find some additional trigger for the longest events. Such long events correspond to the most damped collisions with the formation of mostly excited primary fragments decaying by fission, see figures 18(a). However, there is also a chance for the production of the primary fragments in the region of doubly magic nucleus ^{208}Pb, which could survive against fission due to nucleon evaporation. The number of the longest events depends weakly on impact parameter up to some critical value. On the other hand, in the angular distribution of all the excited primary fragments (strongly peaked at the centre-of-mass angle slightly larger than 90°) there is the rapidly decreasing tail at small angles, see figure 18(b). Time distribution for the most damped events

($E_{loss} > 150$ MeV) in which a large mass transfer occurs and primary fragments scatter in forward angles ($\theta_{c.m.} < 70^\circ$) is rather narrow and really shifted to longer time delay; see hatched areas in figure 17.

For the considered case of ^{238}U+^{248}Cm collision at 800 MeV centre-of-mass energy, the detection of the surviving nuclei in the lead region at the laboratory angles of about 25° and at the low-energy border of their spectrum (around 1000 MeV for Pb) could be a real trigger for longest reaction time.

5. Conclusion

For near-barrier collisions of heavy ions it is very important to perform a combined (unified) analysis of all strongly coupled channels: deep-inelastic scattering, quasi-fission, fusion and regular fission. A unified potential energy surface is derived determining the evolution of the nuclear system in all the channels. This potential has appropriate values of the Coulomb barriers in the entrance channel and proper values of the fission barriers in the exit one. A unified set of dynamic Langevin-type equations is proposed for the simultaneous description of DI and fusion–fission processes. For the first time, the whole evolution of the heavy nuclear system can be traced starting from the approaching stage and ending in DI, QF and/or fusion–fission channels. Satisfactory agreement of our calculations with experimental data gives us hope not only to obtain rather accurate predictions of the probabilities for super-heavy element formation but also to clarify much better than before the mechanisms of quasi-fission and fusion–fission processes. Also the determination of such fundamental characteristics of nuclear dynamics as the nuclear viscosity and the nucleon transfer rate is now possible.

The production of long-lived neutron-rich SH nuclei in collisions of transuranium ions seems to be quite possible due to a large mass and charge rearrangement in the inverse (anti-symmetrized) quasi-fission process caused by the $Z = 82$ and $N = 126$ nuclear shells. Radiochemical identification of ^{267,268}Db and ^{271,272}Bh isotopes, produced in the Th+Cf or U+Cm reactions, could be performed, for example, to test this conclusion. If the found cross sections will be higher than several picobarns, then the subsequent experiments with such reactions could be planned aimed to the production of SH nuclei just in the region of the 'island of stability'. Parallel search for spontaneous positron emission from a super-critical electric field of long-living giant quasi-atoms formed in these reactions is also quite promising.

Acknowledgments

The work was supported partially by the DFG-RFBR collaboration project under grant no 04-02-04008 and by INTAS, grant no 03-51-6417.

References

[1] Schröder W U and Huizenga J R 1984 Damped nuclear reactions *Treatise on Heavy-Ion Science* vol 2 ed D A Bromley (New York: Plenum) p 140

[2] Hulet E K, Lougheed R W, Wild J F, Landrum J H, Stevenson P C, Ghiorso A, Nitschke J M, Otto R J, Morrissey D J, Baisden P A, Gavin B F, Lee D, Silva R J, Fowler M M and Seaborg G T 1977 *Phys. Rev. Lett.* **39** 385

[3] Schädel M, Kratz J V, Ahrens H, Brüchle W, Franz G, Gäggeler H, Warnecke I, Wirth G, Herrmann G, Trautmann N and Weis M 1978 *Phys. Rev. Lett.* **41** 469

[4] Freiesleben H, Hildenbrand K D, Pühlhofer F, Schneider W F W, Bock R, Harrach D V and Specht H J 1979 *Z. Phys.* A **292** 171

[5] Schädel M, Brüchle W, Gäggeler H, Kratz J V, Sümmerer K, Wirth G, Herrmann G, Stakemann R, Tittel G, Trautmann N, Nitschke J M, Hulet E K, Lougheed R W, Hahn R L and Ferguson R L 1982 *Phys. Rev. Lett.* **48** 852
[6] Moody K J, Lee D, Welch R B, Gregorich K E, Seaborg G T, Lougheed R W and Hulet E K 1986 *Phys. Rev.* C **33** 1315
[7] Welch R B, Moody K J, Gregorich K E, Lee D, Seaborg G T, Lougheed R W and Hulet E K 1987 *Phys. Rev.* C **35** 204
[8] Mayer W, Beier G, Friese J, Henning W, Kienle P, Körner H J, Mayer W A, Müller L, Rosecondnameer G and Wagner W 1985 *Phys. Lett.* B **152** 162
[9] Hofmann S and Münzenberg G 2000 *Rev. Mod. Phys.* **72** 733
[10] Oganessian Yu Ts, Utyonkov V K, Lobanov Yu V, Abdullin F Sh, Polyakov A N, Shirokovsky I V, Tsyganov Yu S, Gulbekian G G, Bogomolov S L, Gikal B N, Mezentsev A N, Iliev S, Subbotin V G, Sukhov A M, Voinov A A, Buklanov G V, Subotic K, Zagrebaev V I, Itkis M G, Patin J B, Moody K J, Wild J F, Stoyer M A, Stoyer N J, Shaughnessy D A, Kenneally J M, Wilk P A, Lougheed R W, Il'kaev R I and Vesnovskii S P 2004 *Phys. Rev.* C **70** 064609
[11] Péter J, Ngô C, Plasil F, Tamain B, Berlanger M and Hanappe F 1977 *Nucl. Phys.* A **279** 110
[12] Itkis M G, Oganessian Yu Ts, Bogatchev A A, Itkis I M, Jandel M, Kliman J, Kniajeva G N, Kondratiev N A, Korzyukov I V, Kozulin E M, Krupa L, Pokrovski I V, Prokhorova E V, Pustylnik B I, Rusanov A Ya, Voskresenski V M, Hanappe F, Benoit B, Materna T, Rowley N, Stuttge L, Giardina G and Moody K J 2001 *Proc. Fusion Dynamics at the Extremes (Dubna, 2000)* ed Y T Oganessian and V I Zagrebaev (Singapore: World Scientific) p 93
[13] Itkis M G, Äystö J, Beghini S, Bogatchev A A, Corradi L, Dorvaux O, Gadea A, Giardina G, Hanappe F, Itkis I M, Jandel M, Kliman J, Khlebnikov S V, Kniajeva G N, Kondratiev N A, Kozulin E M, Krupa L, Latina A, Materna T, Montagnoli G, Oganessian Yu Ts, Pokrovski I V, Prokhorova E V, Rowley N, Rubchenya V A, Rusanov A Ya, Sagaidak R N, Scarlassara F, Stefanini A M, Stuttge L, Szilner S, Trotta M, Trazaska W H, Vakhtin D N, Vinodkumar A M, Voskresenski V M and Zagrebaev V I 2004 *Nucl. Phys.* A **734** 136
[14] Berriman A C, Hinde D J, Dasgupta M, Morton C R, Butt R D and Newton J O 2001 *Nature* **413** 144
[15] Zagrebaev V and Greiner W 2005 *J. Phys. G: Nucl. Part. Phys.* **31** 825
[16] Reinhardt J, Müller U and Greiner W 1981 *Z. Phys.* A **303** 173
[17] Greiner W (ed) 1983 *Quantum Electrodynamics of Strong Fields* (New York and London: Plenum)
Greiner W, Müller B and Rafelski J 1985 *QED of Strong Fields* 2nd edn (Berlin: Springer)
[18] Blocki J, Randrup J, Swiatecki W J and Tsang C F 1977 *Ann. Phys., NY* **105** 427
[19] Bass R 1980 *Nuclear Reactions with Heavy Ions* (Berlin: Springer) p 326
[20] Zagrebaev V I, Itkis M G and Oganessians Yu Ts 2003 *Phys. At. Nucl.* **66** 1033
Zagrebaev V I, Itkis M G and Oganessians Yu Ts 2003 *Yad. Fiz.* **66** 1069
[21] Gontchar I I, Dasgupta M, Hinde D J, Butt R D and Mukherjee A 2002 *Phys. Rev.* C **65** 034610
[22] Zagrebaev V I and Samarin V V 2003 *Phys. At. Nucl.* **67** 1462
Zagrebaev V I and Samarin V V 2004 *Yad. Fiz.* **67** 1488
[23] Scheid W, Ligensa R and Greiner W 1968 *Phys. Rev. Lett.* **21** 1479
[24] Diaz-Torres A 2004 *Phys. Rev.* C **69** 021603
[25] Zagrebaev V I and Samarin V V 2006 *Yad. Fiz.* at press
[26] Zagrebaev V I 2001 *Phys. Rev.* C **64** 034606
[27] Zagrebaev V I 2004 *Tours Symposium on Nuclear Physics AIP Conf. Proc.* ed M Arnould *et al* No. 704 (Melville, NY: AIP) p 31
[28] Mosel U, Maruhn J and Greiner W 1971 *Phys. Lett.* B **34** 587
Maruhn J and Greiner W 1972 *Z. Phys.* **251** 431
[29] Sierk A J 1986 *Phys. Rev.* C **33** 2039
[30] Möller P, Nix J R, Myers W D and Swiatecki W J 1995 *At. Data Nucl. Data Tables* **59** 185
[31] Myers W D and Swiatecki W 1974 *Ann. Phys., NY* **84** 186
[32] Fröbrich P and Gonchar I I 1998 *Phys. Rep.* **292** 131
[33] Dasgupta M, Hinde D J, Rowley N and Stefanini A M 1998 *Annu. Rev. Nucl. Part. Sci.* **48** 401
[34] Nishio K, Ikezoe H, Mitsuoka S and Lu J 2000 *Phys. Rev.* C **62** 014602
Mitsuoka S, Ikezoe H, Nishio K and Lu J 2000 *Phys. Rev.* C **62** 054603
[35] Werner F G and Wheeler J A, unpublished
Davies K T R, Sierk A J and Nix J R 1976 *Phys. Rev.* C **13** 2385
[36] Nörenberg W 1974 *Phys. Lett.* B **52** 289
[37] Moretto L G and Sventek J S 1975 *Phys. Lett.* B **58** 26

[38] Ayik S, Schürmann B and Nörenberg W 1976 *Z. Phys.* A **279** 174
[39] Schmidt R and Wolschin G 1980 *Z. Phys.* A **296** 215
[40] Zagrebaev V I 2003 *Phys. Rev.* C **67** 061601
[41] Eisenberg J H and Greiner W 1970 *Nuclear Theory (Nuclear Models vol 1)* (Amsterdam: North Holland)
Bohr A and Mottelson B R 1974 *Nuclear Structure (Nuclear Deformations vol 2)* (New York: Benjamin)
[42] Hilscher D and Rossecondnameer H 1993 *Proc. Int. School–Seminar on Heavy Ion Physics (Dubna, 1993)* ed Yu Ts Oganessian *et al* (JINR, Dubna) p 230
[43] Gross D H E and Kalinowski H 1974 *Phys. Lett.* B **48** 302
[44] Davies K T R, Managan R A, Nix J R and Sierk A J 1977 *Phys. Rev.* C **16** 1890
[45] Randrup J and Swiatecki W J 1984 *Nucl. Phys.* A **429** 105
[46] Feldmeier H 1987 *Rep. Prog. Phys.* **50** 915
[47] Hofmann H 1997 *Phys. Rep.* **284** 137
Ivanyuk F A 2000 *Proc. Dynamical Aspects of Nuclear Fission (Slovakia, 1998)* ed Yu Ts Oganessian, J Kliman and S Gmuca (Singapore: World Scientific) p 424
[48] Zagrebaev V I, Aritomo Y, Itkis M G, Oganessian Yu Ts and Ohta M 2002 *Phys. Rev.* C **65** 014607
[49] Wilcke W W, Birkelund J R, Hoover A D, Huizenga J R, Schröder W U, Viola V E Jr, Wolf K L and Mignerey A C 1980 *Phys. Rev.* C **22** 128
[50] Itkis M G 2005 private communication
[51] Bürvenich T *et al* 2004 *Phys. Rev.* C **69** 014307
[52] Zagrebaev V I, Itkis M G, Oganessian Yu Ts and Greiner W 2006 *Phys. Rev.* C **73** 031602
[53] Ahmad I, Austin Sam M, Back B B, Betts R R, Calaprice F P, Chan K C, Chishti A, Conner C M, Dunford R W, Fox J D, Freedman S J, Freer M, Gazes S B, Hallin A L, Happ Th, Henderson D, Kaloskamis N I, Kashy E, Kutschera W, Last J, Lister C J, Liu M, Maier M R, Mercer D M, Mikolas D, Perera P A A, Rhein M D, Roa D E, Schiffer J P, Trainor T A, Wilt P, Winfield J S, Wolanski M, Wolfs F L H, Wuosmaa A H, Young A R and Yurkon J E (APEX Collaboration) 1999 *Phys. Rev.* C **60** 064601
[54] Ganz R, Bär R, Balanda A, Baumann J, Berg W, Bethge K, Billmeier A, Bokemeyer H, Fehlhaber H, Folgera H, Foryciara J, Fröhlich O, Hartung O, Rhein M, Samek M, Salabura P, Schön W, Schwalm D, Stiebing K E and Thee P (EPoS II Collaboration) 1996 *Phys. Lett.* B **389** 4
[55] Leinberger U, Berdermanna E, Heine F, Heinz S, Joeres O, Kienle P, Koenig I, Koenig W, Kozhuharov C, Rhein M, Schröter A and Tsertos H (ORANGE Collaboration) 1997 *Phys. Lett.* B **394** 16
[56] Mittig W, Heinz S and Villari A C C 2005 *Proposal for GANIL Experiment*
[57] Greiner W, Park Jae Y and Scheid W 1995 *Nuclear Molecules* (Singapore: World Scientific)
[58] Riedel C and Nörenberg W 1979 *Z. Phys.* A **290** 385
[59] Maruyama T, Bonasera A, Papa M and Chiba S 2002 *Eur. Phys. J.* A **14** 191